Colloids and Surfaces B: Biointerfaces 193 (2020) 111124

Contents lists available at ScienceDirect

Colloids and Surfaces B: Biointerfaces

journal homepage: www.elsevier.com/locate/colsurfb

Arthrospira platensis transglutaminase derived antioxidant peptide-packed electrospun chitosan/ poly (vinyl alcohol) nanofibrous mat accelerates wound healing, *in vitro*, via inducing mouse embryonic fibroblast proliferation

Anbazahan Sannasimuthu[a], Madhura Ramani[a], Bilal Ahamad Paray[b], Mukesh Pasupuleti[c], Mohammad K. Al-Sadoon[b], Tamil Selvi Alagumuthu[d], Abdul Rahman Al-Mfarij[b], Aziz Arshad[e,f], Kanchana Mala[g,*], Jesu Arockiaraj[h,*]

[a] Department of Biotechnology, Faculty of Science and Humanities, SRM Institute of Science and Technology, Kattankulathur 603 203, Chennai, Tamil Nadu, India
[b] Department of Zoology, College of Science, King Saud University, PO Box 2455, Riyadh, 11451, Saudi Arabia
[c] Lab PCN 206, Microbiology Division, CSIR-Central Drug Research Institute, B.S. 10/1, Sector 10, Jankipuram Extension, Sitapur Road, Lucknow, 226 031, Uttar Pradesh, India
[d] Unit for Science Dissemination (UDS), CSIR-Central Leather Research Institute, Adyar, Chennai, 600 020, India
[e] International Institute of Aquaculture and Aquatic Sciences (I-AQUAS), Universiti Putra Malaysia, 71050, Port Dickson, Negeri Sembilan, Malaysia
[f] Department of Aquaculture, Faculty of Agriculture, Universiti Putra Malaysia, 43400, Serdang, Selangor, Malaysia
[g] Medical College Hospital and Research Center, SRM Institute of Science and Technology, Potheri, 603203, Tamil Nadu, India
[h] SRM Research Institute, SRM Institute of Science and Technology, Kattankulathur, 603 203, Chennai, Tamil Nadu, India

ARTICLE INFO

Keywords:
Arthrospira platensis
Electrospinning
Antioxidant peptide
Chitosan
Polyvinyl alcohol
Wound healing

ABSTRACT

In this present study, we have carried out the antioxidant function of transglutaminase (TG) identified from *Arthrospira platensis* (*Ap*) transcriptome. The antioxidant peptide ML11 (MLRSIGIPARL) has been predicted from the transglutaminase core domain and the peptide's free radical scavenging potential was evaluated and it shows that it functions on a dose dependent manner. The ML11 peptide cell toxicity was analysed in the human blood leucocytes which resulted no cytotoxic activity in any of the cell population. Moreover, the nanofibre mat encapsulated with antioxidant peptide ML11 was prepared by electrospinning technique. The antioxidant peptide ML11 encapsulated mat showed increase in fibre diameter compared to the chitosan polyvinyl alcohol blended mat. The change in the crystalline behaviour of both chitosan and polyvinyl alcohol polymer to the amorphous nature was determined by X-ray diffraction at the broad band between 20 and 30° (2θ°). FTIR revealed the functional groups which present in the polymer as well as the interaction between their components of chitosan (CS) and polyvinyl alcohol (PVA). The fibre retains the antioxidant activity due to the peptide encapsulated by scavenging the intracellular ROS that was confirmed by flowcytometry and fluorescence microscopy. The ML11 peptide encapsulated mat showed no cytotoxicity in the NIH-3T3 mouse embryonic fibroblast cells. Also, ML11 peptide encapsulated fibre showed potential wound healing activity in NIH-3T3 cells. Taken altogether, the study indicates that the wound healing potential of the ML11 peptide encapsulated nano fibre mat may be used as biopharmaceutical drug.

1. Introduction

Skin is one of the largest organs of the body which protects the internal organs against infection, heat or injury and it involves in various functions such as protection, immunity, temperature control, metabolism, communication, fluid hemostasis, sensory detection and self-healing [1]. A chronic wound or skin ulcers can be caused by accidental injury, tumor, diabetic mellitus and skin burns or venous stasis. Wound healing is the complex process, dynamic and interactive mechanism and involves the array of variants, cytokines, growth factors, extra cellular matrix, blood cell and parenchymal cells [2,3]. Wound healing process can be divided into four phases; hemostasis, inflammatory, proliferation and maturation or remodelling [4]. Reactive oxygen species (ROS) plays a crucial role in the wound healing process where,

* Corresponding authors.
E-mail addresses: kanchana39@gmail.com (K. Mala), jesuaraj@hotmail.com (J. Arockiaraj).

https://doi.org/10.1016/j.colsurfb.2020.111124
Received 29 January 2020; Received in revised form 3 May 2020; Accepted 7 May 2020
Available online 13 May 2020

during inflammatory phase, the immune cells like neutrophils and macrophage migrate towards the wound site and starts to trigger the ROS production.

However, the normal level of ROS at the wound site, prevents the invasion of bacterial pathogens or infection and the moderate level of ROS participates in re-epithelialization by initiating the production of keratinocyte and epidermal growth factor receptors. When increasing the ROS level at the wound site, it can drastically damage the affected tissues as well as neighbouring healthy tissues; also elevated ROS decelerates the angiogenesis which may lead to cell death. The excess level of ROS can halt the fast healing of wound and it can be caused by several factors like environmental, physical or induced oxidative stress [5]. Oxidative stress by both radical and non-radical ROS may prevent the proliferation and migration of the cells during the wound closure process [6,7].

In skin ulcers, the exudates production lead to the maceration of healthy skin and halts the wound healing process [8]. Now a day's numerous researchers have interested to treat the wound by bio scaffolds. The recent study reported that the use of bio scaffolds in the treatment of wound is due to its bacterial protection, biocompatibility, biodegradable, epithelization at the wound site, high surface area to volume ratio, high porosity and low cost [9]. The fabrication of the scaffold can be achieved by electrospinning method due to its property of controlled pore size, very large surface area to volume ratio, versatility, reproducibility and submicron range have been used in the biomedical application [10]. The polymeric nature of the nanofibrous mat has the ability to heal the wound due to its regeneration and repair capability [9]. Interestingly, chitosan polymer has been reported to form hydrogel, fibres, scaffolds and membranes. It reduces the bleeding and reduces the pain by blocking the nerve endings [11]. The electro spun nanofibre of chitosan has been widely used as the wound dressing due to its properties such as oxygen permeability, high porosity, and variation in pore size which can prevent the exudates and help in the fast healing of wound.

Hence, it is an important to identify the novel drug to treat the wound affected by the oxidative stress particularly ROS. An approach to improve the fast healing of the wound is to tune or control the excess level of oxidative stress with the help of antioxidant enzyme which would escalates the healing process [12]. The present study is focused on reducing the elevated level of ROS during the wound healing process by fabricated nanofibrous mat loaded with enzymatic derived antioxidant peptide. From the established *A. platensis* transcriptome database, a complete cDNA sequence of transglutaminase (*Ap*TG) was identified. Gene expression analysis was achieved to understand the *Ap*TG antioxidant role during H_2O_2 oxidative stress. A short peptide sequence has been identified from *Ap*TG core domain. Physicochemical parameters of the amino acids included compositions, arrangement of sequence, structure, molecular weight and hydrophobicity represented that the peptide has intracellular free radical scavenging activity. The ML11 peptide has been synthesized chemically and its free radical scavenging ability was evaluated by cell-free assays and *in vitro* assays. Also, The ML11 peptide cell toxicity analysis has been performed to human peripheral blood mononuclear cells (PBMCs) and the peptide was checked during H_2O_2 exposed blood leucocytes, the intracellular ROS level modulation was determined by FACS and fluorescence microscopy. Furthermore, utilizing electrospinning technique, peptide loaded nanofiber mat was fabricated. The morphology of the nanofibre mat was observed using SEM, X-ray diffraction and IR- spectroscopy analysis. Finally, the *in vitro* study demonstrated that the peptide ML11 involved in proliferation and migration of NIH-3T3 cells which was confirmed microscopically.

2. Materials and methods

2.1. Blue-green algae cultivation

The single cell organism spirulina were collected and cultivated as mentioned in the earlier manuscript [13]. The isolated blue-green algae have been identified as *A. platensis* by gene sequencing (16S rRNA) and evolutionary analysis and the gene sequence has been deposited in National Institutes of Health (NIH) genetic sequence database, NCBI GenBank under the accession ID: KY393096.

2.2. H_2O_2 challenge and spirulina cell collection

In order to find out the influence of H_2O_2 stress on *A. platensis*, the algal cells were cultivated in two different conditions: i) cells treated with H_2O_2 (10 mM concentration = 30% H_2O_2 w/w in H_2O) ii) cells untreated with H_2O_2 maintained as control. Both the challenged and control group, the cells were collected in a consistent period (day 0, 5, 10, 15 and 20) as described in our earlier manuscript [13] and immediately stored at deep freezer for further study. Both the challenged and control cells were taken for analysis in triplicate at various time points.

2.3. RNA extraction, cDNA conversion and gene expression study

The algal cells were collected from both treated and untreated group of the spirulina cells were used for the isolation of total RNA by TRIzol reagent method. Then, utilizing Transcriptor First Strand cDNA Synthesis Kit (Roche Diagnostics GmbH, Germany) cDNA was obtained from the RNA as described in our earlier manuscript [13]. Followed by the *Ap*TG gene were amplified using cDNA as template with the respective primers (E-Suppl. Table 1). For the assay, 16 s rRNA was used as reference gene.

2.4. In silico characterization of ApTG

From the spirulina transcriptome, a complete *Ap*TG cDNA sequence has been identified which was obtained by Illumina NextSeq500 technology as described in our previous manuscript [14]. The identified *Ap*TG cDNA sequence was deposited to the EMBL (European Molecular Biology Laboratory) archive. Further, similarity search, multiple sequence alignment, molecular mass, theoretical isoelectric point (pI), aliphatic index, instability index, domain and motif analysis and three-dimensional structure of the of *Ap*TG protein was analysed using different available online software such as Prosite, ProtParam and BLAST.

2.5. Identification and synthesis of antioxidant peptide

Several factors determine the antioxidant property which include, amino acid compositions, arrangement of sequence, molecular mass, evolutionary conserved region and hydrophobicity nature [15]. Antioxidant peptide sequence MLRSIGIPARL (ML11) was determined from *A. platensis* transglutaminase core domain of the protein. An online tool PEPTIDE 2.0 was used to analyse the hydrophobicity and hydrophilicity property of the short peptide ML11. The amphipathic nature of ML11 peptide has been predicted using online tool. Further, the peptide ML11 was synthesized (Zhengzhou Peptides Pharmaceutical Technology Co., Ltd) and purity was measured as 99.73% by HPLC and it was confirmed by MALDI-TOF MS analysis. For the further work, peptide was dissolved in endotoxin free water and maintained as a stock in 1 mM concentration which was stored at −20°C.

2.6. In vitro cell-free antioxidant assays

Various cell-free antioxidant assays were performed to determine the ML11 peptide free radical scavenging activity. The following assays

such as 2,2-diphenyl-1-picrylhydrazyl (DPPH), 2,2′-azino-bis 3-ethylbenzothiazoline-6-sulfonic acid (ABTS), hydroxyl and superoxide anion free radical scavenging assays with slight modifications as described in our previous manuscript [16]. Trolox has been used as positive control. The free radical scavenging activities were calculated as:

$$\text{Free radical scavenging activity} = \frac{\text{A control} - \text{A sample}}{\text{A control}} \text{X } 100\%$$

2.7. Determination of intracellular ROS in human PBMCs by DCFDA

To determine the intracellular ROS level, DCFDA dye was used [17]. Briefly, the level of intracellular ROS has been measured using cell-permeable fluorescent probe 2′,7′-dichlorofluorescein diacetate (DCFDA).

2.8. Cell toxicity of ML11 on human PBMCs

Cell toxicity effect using PBMCs from healthy human (Ethical Clearance No. CDRI/IEC/2014/A1) was investigated using ML11 peptide. The assay has been conducted as described in our previous finding [13]. All the tests were done in triplicates and the results were expressed as mean ± standard deviation. This study complies with the Declaration of Helsinki.

2.9. Preparation of nanofiber mat using electrospinning method

Chitosan (CS) (mol. wt. 150,000 Da) of 2% w/v was dissolved in 1% acetic acid and stirred under constant stirring at 37 °C for 5–6 h. Polyvinyl alcohol solution (PVA) (mol. wt. 85,000 Da of 12% w/v was prepared by dissolving polyvinyl alcohol in deionised water at 80°c for 5 h under constant stirring. Both CS and PVA solutions were blended together at three different weight ratios of 1: 3, 1.5: 3 and 2: 3. The peptide at 1 mM concentration was added to the blended polymer solution. Further, the electrospinning parameters were optimized and the voltage of 15 kV were supplied in a 12 cm distance that was calculated between the collector and the tip of the needle. The flow rate of the polymer was set at 0.2 ml/h. The fabricated mats were prepared by electrospinning method as described previously [18,19].

2.10. Characterization of nanofiber mat

2.10.1. SEM analysis

FE-SEM method was used in the characterization study to determine the morphology of electrospun nanofiber and the average diameter of the fibres were measured using an image analysis software ImageJ [20,21].

2.10.2. FTIR analysis

Fourier transform infrared spectroscopy studies were performed to confirm the functional groups present in the polymers and the interaction between the components of CS and PVA. FTIR was performed in ATR mode (attenuated total reflection) in the wavelength range of 400 – 4000 cm^{-1} with 45 scans at the resolution of 2 cm^{-1}.

2.10.3. XRD analysis

In order to study the physical properties of chitosan and polyvinyl nanofiber mats, the X-ray diffraction technique was performed with the Cu kα radiation wavelength of 0.154 nm. The pattern determined at the voltage of 40 kV and current of 15 mA with over the range of 5°- 100° (2 theta degree).

2.11. Loading capacity of ML11 peptide

The release kinetics of the peptide highly depends on the loading capacity in the fabricated nanofiber [22]. As chitosan is a hydrophobic polymer and PVA is a hydrophilic polymer, it was not possible to dissolve the mat either in water or acetic acid, so we have chosen PBS to dissolve. To remove the polymeric interference in collecting the peptide for standard calibration curve, we centrifuge it and collected the supernatant that containing peptide. To determine the loading capacity of the peptide, the nanofibrous mat (6 mg) were weighed and centrifuged at 2000 rpm for 10 min and the supernatant was collected to measure the optical density at 260 nm using UV-VIS spectrophotometer [10,27]. The loading capacity of the peptide in the nanofibrous mat was calculated as following formula:

$$\text{Loading capacity \%} = \frac{\text{Actual peptide amount}}{\text{Weight of fibres}} \text{X } 100$$

2.12. Encapsulation efficiency of ML11 peptide

The efficient encapsulation of peptide into the polymer mat were measured using the encapsulation efficiency method. The study was conducted as reported in similar study with slight modifications [23]. The peptide loaded mat were subjected to centrifugation at 2000 rpm for 10 min and the resulting supernatant was measured using UV-VIS spectrophotometer at 260 nm. While centrifuge the peptide loaded polymeric mat, the peptide may be released in the medium or supernatant and the pellet we obtained contained polymers. Percentage of encapsulation efficiency was calculated as following formula:

$$\text{Encapsulation efficiency \%} = \frac{\text{Actual peptide amount}}{\text{Theoretical peptide amount}} \text{X } 100$$

2.13. In vitro drug release study

The drug release study was performed to evaluate the amount of peptide released from the nanofiber mat as reported [10]. The mats were cut into small pieces (1 cm × 1 cm) and immersed in 5 ml of phosphate buffer saline solution (pH 7.4), which was incubated overnight at 37°C under shaking condition. The release media of 1 ml was read at 260 nm using UV–vis spectrophotometer. The readings were taken at different time intervals starting from the zero hour. To calculate the cumulative release percentage of the peptide released from the mat, the following equation was used;

$$\text{Cumulative release} = \frac{\text{Total amount of drug released from the mat}}{\text{Total amount of drug loaded initially}} \text{X } 100$$

2.14. Intracellular ROS level determination using DCFDA

In this study, the antioxidant peptide loaded nanofiber mat was used to determine the free radical scavenging property against oxidative stress induced PBMCs. The production of oxidative stress in the leucocytes can be measured using DCFDA dye. Once the cells take up the DCFDA dye, it is deacetylated to a non-fluorescent compound which oxidize to a fluorescent compound dichlorofluorescein (DCF) by the oxidative stress present in the cell [24,25]. In brief, the level of intracellular ROS has been quantified using 20 μM DCFDA dye. Further studies were performed to confirm the free radical scavenging activity of the ML11 peptide loaded nanofiber mat using the confocal fluorescence microscopy.

2.15. MTT assay

MTT assay was performed based on the standard procedure adapted from ISO10993-5 [26,27] to determine the viability of NIH-3T3 (National Centre for Cell Science, Pune) cells against the ML11 peptide loaded nanofiber. In brief, the peptide mat of 5 mg was sterilized under UV radiation for 10 min. and dissolved in serum free Dulbecco's modified eagle medium (DMEM) for 24 h in a sterile condition. NIH-3T3

cells were seeded into the 96 well plate and maintained in DMEM along with 10% FBS, at a density of 1 × 10^5 cells/well and the cells were maintained at 37 °C for 24 h in 5% CO_2 condition. Followed by incubation cells were treated with and without peptide loaded nanofiber. After 24 h of incubation, the MTT reagent of 20 µl was added to wells and kept for 4 h of incubation at 37 °C. Finally, the MTT reagents were removed and 200 µl of DMSO was added to dissolve the formazan crystals formed. The absorbance of the sample was measured at 570 nm using an ELISA reader.

2.16. Scratch assay

The scratch assay was performed to determine the wound closure activity of the ML11 peptide loaded mats in the NIH-3T3 cells. The study was conducted as reported by Tsai et al, with slight modifications [28]. Mouse fibroblast cells (NIH-3T3) were procured from cell culture center of National Centre for Cell Science, Pune. The NIH-3T3 cells were seeded at a density of 8 × 10^5 cells/well into a 6-well plate and the cells were maintained at 37 °C in a humidified atmosphere of 5 % CO_2 condition. After the incubation period, media was completely removed. In the middle of cell monolayer, a scratch was made by P10 sterile pipette tip to mimic the wound. Further, treatments were added to both controls and samples and the plate was incubated for 24 h. The cells grown in extract free medium were used as control. The wound was exposed to ML11 peptide loaded nanofiber mat for 24–72 h time interval. Scratch wound closure was analysed under the inverted microscope (Magnus INVI, Noida) equipped with a digital CCD camera. The wound closure was calculated as following formula;

$$\% = \frac{\text{distance within the scratch at 0 h} - \text{distance within the scratch at 24 h}}{\text{distance within the scratch at 0 h}} \times 100$$

2.17. Statistical analysis

Statistical value of the given data was analysed using two-way ANOVA and Sidak's test in GraphPad prism (version 8.0.2) with the significance value indicated as p which was less than 0.05. All the assays were performed in triplicates and were performed to determine the mean and standard deviation. Results were reported as mean of three independent experiments ± SD.

3. Results and discussion

3.1. ApTG mRNA expression analysis during H_2O_2 stress

The *Ap*TG mRNA expression was quantified using the cDNA as a template along with other necessary reaction mixtures including primers in RT-PCR. *Ap*TG mRNA was expression was significantly ($P < 0.05$) induced on day 15 due to the exposure of 10 mM H_2O_2. Also, H_2O_2 exposure induced significant raise in expression level of *Ap*TG at the initial point of exposure when contrast to the final point where there was a steady reduction in expression, which has been noticed as an indication that the *Ap*TG expression was returned to its basal level (Fig. 1). It has been demonstrated that the role of transglutaminase 2 in apoptosis induced by H_2O_2 in human chondrocytes are found in cartilage connective tissue revealing the antioxidant role of transglutaminase against H_2O_2 [29]. This indicated that *Ap*TG was significantly involved in protecting the cells from oxidative damage and it played a pivotal role in antioxidant activities.

3.2. Identification and sequence analysis of ApTG

From the transcriptome database, A complete cDNA sequence encoding *Ap*TG has been identified and submitted to EMBL (European Molecular Biology Laboratory) archive with the accession ID.

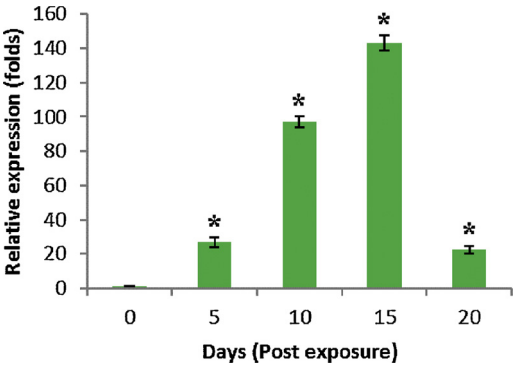

Fig. 1. Gene expression profiling of *Ap*TG post treatment with H_2O_2. The modulated expression of transglutaminase post H_2O_2 challenge in *A. platensis* measured by qRT-PCR at various times (0, 5, 10, 15 and 20 days). On 15^{th} day of post-treatment (p.t.) the elevated expression of *Ap*TG mRNA was found and the reduction of expression was observed at 20^{th} day of p.t. The asterisk (*) refers the significant different between control (day 0) and treatments (day 5, 10, 15 and 20) by two-way ANOVA and Sidak's test in GraphPad prism (version 8.0.2).

LT667401. The full length *Ap*TG cDNA sequence contained 4861 nucleotide base pairs (bps). The ProtParam results revealed that the *Ap*TG protein possessed a calculated isoelectric point (pI) of 9.16 and their predicted molecular weight was found to be 88,824.5 Da. In addition, the *Ap*TG protein sequence has positive (Arginine + Lysine) and negative (Aspartic acid + Glutamic acid) charged residues, which are 81 and 72 residues, respectively. The aliphatic index of the protein *Ap*TG was calculated to be 99.51 which indicate that the protein reveals better thermostability due to the presence of aliphatic amino acids such as alanine, valine, leucine and isoleucine in the *Ap*TG protein. The cellular localization prediction analysis of *Ap*TG on MultiLoc2 online tool demonstrated that the *Ap*TG is localized in mitochondria.

In addition, the CDD result disclosed that the *Ap*TG possessed three distinct domains. Of these, the transglutaminase core domain (pfam01841) present in *Ap*TG C-terminal end which is located between ^{471}T-P^{588} and other two presumed domains present in both N-terminal (pfam11992) and C-terminal end (pfam13559) which is located between ^{35}L-G^{224} and ^{695}L-E^{765}, respectively. The multiple sequence alignment also showed that the residues which are conserved with other homologous sequences. But *Ap*TG sequence does not remain conserved with animals and humans. A large number of significant residues were evolutionarily conserved and the aligned sequence was represented in the E-Suppl. Fig. 1A.

3.3. Tertiary structure analysis of ApTG

The tertiary structure analysis of *Ap*TG protein also confirmed that the result obtained during the secondary structural analysis such as 62.78% and 37.22% amino acid residues in α-helix and random coil; and 39 and 40 number of distinct α-helices and random coils, respectively (E-Suppl. Fig. 1B). There was no antipleated β-sheet in the structure of *Ap*TG protein. Moreover, the most stable tertiary structure revealed a 'helix-loop-helix' organization. Further analysis of 3D structure showed that the characteristic gene specific transglutaminase core domain is scattered throughout the structure of *Ap*TG protein.

3.4. Molecular characterization of antioxidant peptide ML11

Based on the composition, arrangement, structure, molecular mass and hydrophobicity of amino acids which contribute antioxidant activity, a short peptide sequence ^{537}MLRSGIPARL^{547} (ML11) was predicted from transglutaminase core domain along with conserved amino acid residues and the putative peptide region of the sequence was completely conserved with other cyanobacteria. Particularly, in the

putative peptide regions, the amino acids which were already known to contribute for the antioxidant activity such as M^{537}, $R^{539, 546}$, S^{540} and P^{544} are highly conserved with the other species which shows the importance of those residues in the function of *Ap*TG protein. Further, the molecular weight of the ML11 peptide is measured to be 1226 Da. It has amino acids such as arginine double residues which result with net charge +2 and the isoelectric point is measured to be 12. The amino acid arginine has hydrogen atom which is potentially involved in the antioxidant activity by HAT mechanism. Also, the peptide ML11 exhibited in both hydrophobic and hydrophilic amino acids which is identified that is an amphipathic nature (E-Suppl. Fig. 1C). In addition, the result exhibited that the predicted ML11 peptide was localized in the α-helix (90.90%) together with random coil (09.10%) at the *Ap*TG core domain, C-terminal region (E-Suppl. Fig. 1D).

3.5. Antioxidant mechanism of ML11 peptide on cell-free molecules

3.5.1. DPPH free radical scavenging activity of ML11

In this study, the stable free radical DPPH was applied to assess ML11 peptide free radical scavenging capacity. The peptide ML11 displayed a significant ($P < 0.05$) antioxidant activity at lower dose, when the peptide dose increasing the free radical scavenging activity was increased however the activity was concentration dependent (Fig. 2A). The significant free radical scavenging activity of the ML11 peptide might be due to the presence of Met, Ser, Arg, Pro amino acids. The findings are in agreement with author by Kim et al, where antioxidant peptide ISPRILSYNLR from perila seed protein hydrolysate with lowest molecular weight showed better free radical scavenging activity against DPPH free radical [30]. It has been reported that low molecular mass peptides obtained from *Rhopilema esculentum* hydrolysates exhibited the greatest DPPH free radical scavenging activity [31]. Further, peptide below 3 kDa derived from *Arctoscopus japonicus* has been shown to have the greatest free radical scavenging capacity against DPPH free radical [32]. In addition, low molecular weight peptide disclosed the highest DPPH free radical scavenging activity and also influenced increasing peptide solubility, enabling it to easily bind to the free radical relative with larger, less soluble peptides [33,34]. In correlation with our research, there was potential free radical scavenging activity in ML11 peptide containing hydrophobic amino acids to combat DPPH free radical.

3.5.2. ABTS free radical scavenging activity of ML11

ABTS assay was applied to assess the ML11 peptide antioxidant activity. ABTS free radical was both water soluble and lipid-soluble chemical which is applied to determine the antioxidant activity [35]. It is stated that a single-electron transfer (SET) reaction between ABTS radical cations and amino acids, the labile hydrogen atom, was required to initiate the reaction [36]. So, in this ABTS radical scavenging assay, HAT was considered as a radical scavenger. In this research, ML11 exhibited the ABTS free radical scavenging activity on concentration dependent, where the lower dose of peptide disclosed significant ($P < 0.05$) activity and the increment in peptide concentration exhibited highly increased activity. This free radical quenching potential of ML11 peptide was equivalent to that of trolox (Fig. 2B). A recent finding reported a similar trend, peptides < 2 kDa from fish frame protein hydrolysates disclosed the highest ABTS free radical scavenging activity [37]. Previous study reported that peptides (< 10 kDa) from corn gluten meal showed greatest ABTS free radical scavenging activity

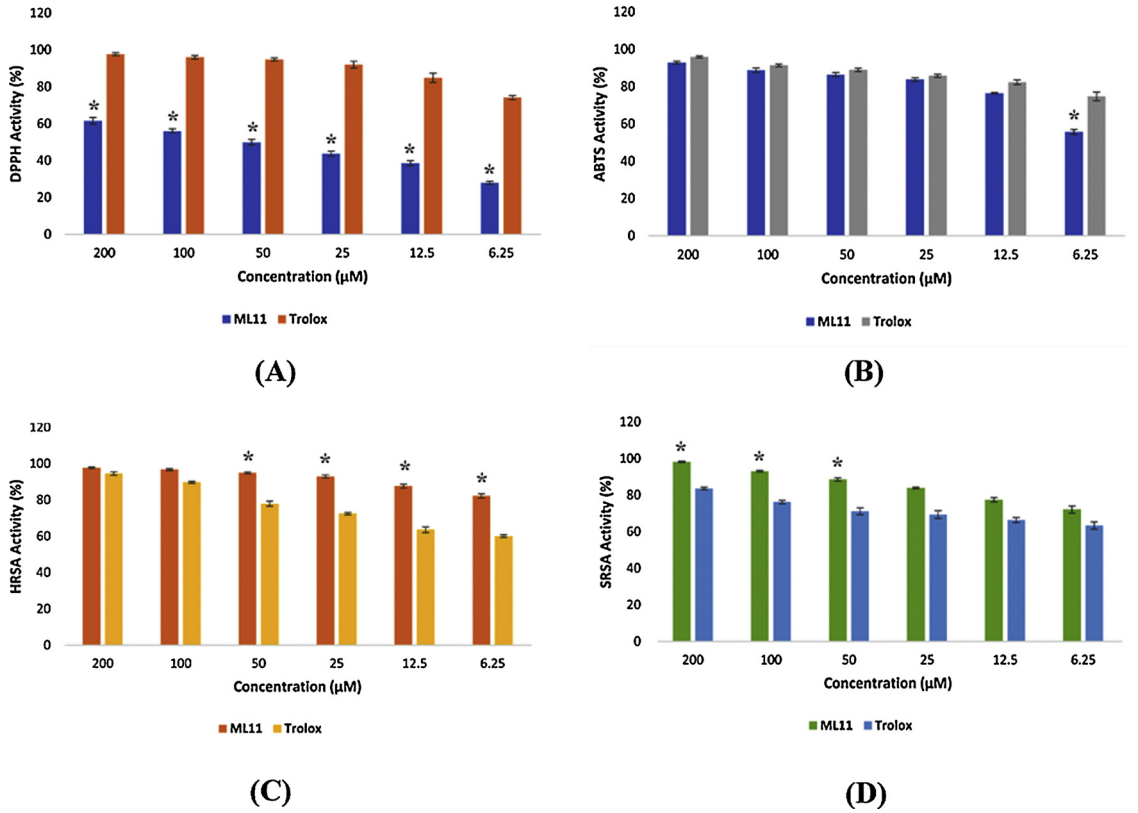

Fig. 2. Antioxidant activity of the ML11 peptide. (A) In comparison with Trolox's DPPH free radical scavenging potentials, ML11 peptide had significant DPPH free radical quenching activity. (B) TEAC assay shows ML11 in the scavenging of ABTS free radicals, the dose dependent trolox-equivalent capacity. (C) HRSA assay displays the capacity of ML11 in quenching of hydroxyl free radicals. (D) Superoxide free radical scavenging activity of ML11 was compared to Trolox, where the free radical scavenging activity of ML11 was superior to Trolox. All tests were conducted in three replicates and the values are represented by the mean ± standard deviation (n = 3). The asterisk (*) denotes the significant difference between positive control (Trolox) and treatments by two-way ANOVA and Sidak's test in GraphPad prism (version 8.0.2).

[38]. These findings indicated that ML11 peptide efficiently involving in the ABTS free radical scavenging activity equivalent to trolox.

3.5.3. Hydroxyl free radical scavenging activity of ML11

In biological systems almost all macromolecules like DNA, RNA, proteins, and polyunsaturated fatty acids are immediately responding with hydroxyl free radicals that trigger severe cell damage [39]. To investigate the hydroxyl free radical quenching capacity of ML11 peptide, o-phenanthroline/H_2O_2 system was used. ML11 exhibited concentration dependent hydroxyl free radical quenching activity, even the lower dose of ML11 peptide exhibited the greater free radical scavenging activity and the higher dose showed drastically increased activity. The free radical scavenging potential of ML11 peptide was higher than trolox (Fig. 2C). A similar study was observed that peptide with lower molecular weight (below 1 kDa) from fermented meat sauce and Jinhua ham possessed better hydroxyl free radical scavenging activity [40,41]. Moreover, Researchers reported that peptide (1471 Da) from duck breast meat showed better free radical scavenging activity against hydroxyl free radical [42]. It has also been reported that hydroxyl and sulfhydryl groups containing amino acids such as serine cysteine and methionine can plays a key role in antioxidant effect [43]. Collectively, our results clearly demonstrated that ML11 peptide has the ability to scavenge the hydroxyl free radical due to the existence of hydroxyl and sulfhydryl groups and lower molecular weight.

3.5.4. Superoxide free radical scavenging activity of ML11

In order to assess the free radical scavenging activity of ML11 peptide, superoxide free radical scavenging assay was performed. By addition of an electron to molecular oxygen, the superoxide radical formed [44,45]. Biomacromolecules include nucleic acids, proteins, carbohydrates and lipids can easily affect by superoxide radical. In this research, ML11 peptide disclosed dose dependent $O_2^{\bullet -}$ free radical quenching activity as observed in other scavenging activities and the greatest antioxidant activity was observed at 200 μM (Fig. 2D). It has been reported that peptides from Spanish dry-cured ham revealed remarkable free radical scavenging activity against superoxide free radicals [46]. Moreover, studies demonstrated that peptide obtained from dry-cured xuanwei ham and duck skin disclosed notable superoxide free radical scavenging activity [47,48]. These observations suggested that ML11 peptide has alleviate the effects of superoxide free radical scavenging activity.

3.6. Intracellular ROS scavenging activity of ML11 in human leucocytes during H_2O_2 stress

It has been proved that H_2O_2 (250 μM) induced human blood leucocytes exhibited highly increased level of intracellular ROS and causes severe damage to the DNA [49]. Therefore, we pursued the intracellular ROS scavenging effect of the ML11 peptide on human blood leucocytes using ROS detecting probe DCFDA. In this study, DCFDA, a non-fluorescent dye diffuses into the cell, it undergoes an enzymatic degradation by intracellular esterase to form DCF fluorescent and this compound is caught within the cells and gets oxidized by H_2O_2. The antioxidant activity of ML11 was assessed on leucocytes as the alleviate level of ROS induced at 30% of H_2O_2. The level of intracellular ROS reduction was noticed in all the analysed sample of ML11 peptide (6.25, 12.5, 25, 50, 100 and 200 μM) in FACS analysis; although ML11 peptide exhibited a significant ($P < 0.05$) antioxidant activity at 25 μM concentrations (Fig. 3A–F). This result confirmed that ML11 peptide disclosed possible ROS scavenging activity in leucocytes and were assessed to be concentration dependent manner. Furthermore, DCFDA stained ML11 peptide treated PBMCs displayed significant intracellular ROS reduction compared to the control cells which was confirmed by fluorescence micrograph analysis (Fig. 3G–J). These findings highlighted the antioxidant activity of ML11 peptide and its inhibition in cellular damage mainly through their intracellular ROS scavenging ability in human blood leucocytes.

3.7. Cell toxicity of ML11 on human PBMCs

It is a well-known fact that the therapeutic peptide does not induce any cytotoxic effect to the host immune cells [50]. Thus, to confirm the ML11 peptide toxicity on human PBMCs, cytotoxicity assay was performed. The results disclosed that ML11 (100 μM) peptide did not induce any substantial toxicity on human PBMCs. The positive control Triton X-100 drastically decreased all the leucocytes cell numbers (Fig. 4). It is clearly indicated that ML11 peptide did not induce cell toxicity against human PBMCs in any of the tested levels. The functional peptide ML11 is therefore human compatible, which could be used as a therapeutic drug for normal cells without any cytotoxic effects.

3.8. Characterization of ML11 peptide encapsulated nanofiber

3.8.1. SEM analysis of ML11 peptide encapsulated nanofiber

The FESEM images of the nanospun fibres showed that all the nanofibers were randomly arranged, continuous with bead free structure and uniform (Fig. 5). In addition, the variations in the electrospinning parameters had no change in the randomness and bead less morphology of the fibers. The average diameter of 1:3 CS-PVA, 1.5:3 CS-PVA and 2:3 CS PVA was found to be 151.6 nm, 234.70 nm and 284.56 nm, respectively. The average fibre diameter increases with the increase in the chitosan concentration in the chitosan-polyvinyl alcohol composite [51]. The smooth and highest diameter fibres was prepared (1.5:3 ratio) to encapsulate the antioxidant peptide [52]. The ML11 peptide loaded mat showed increased fibre diameter which has diameter of 297.80 nm compared to the CSPVA mat. Hosseini et al, reported that the similar increased diameter of fiber was obtained with the incorporation of peptide and this increase in the fibre diameter in the peptide loaded mat must be due to the increase in the viscosity of solution during the addition of peptide [10].

3.8.2. FTIR analysis of ML11 peptide encapsulated nanofiber

The FTIR spectra shows a characteristic band at 3319.12 cm^{-1} (OH stretching), 2844.77 cm^{-1}, and 2908.36 cm^{-1} (CH stretching), 1647.12 cm^{-1} (C═O stretching of amide group), 1555.32cm^{-1} (N—H bending of 1° amine), 1376.25 cm^{-1} (CH_2 bending), 1321.66 cm^{-1} (CH wagging), 1148.52 cm^{-1} (asymmetric bridge of C—O—C bridge), 1028.23 cm^{-1} (C═O stretching) and 888.09cm^{-1} (C—H bending out of plane) corresponding to the chitosan fibres. Whereas, there was a characteristic band at 3288.07 cm^{-1} (O—H stretching), 1733.25 cm^{-1} (due to water absorption), 1424.61 cm^{-1} (CH2 bending), 1321.66 cm^{-1} (CH wagging), 1148.52 cm^{-1} (shoulder stretching of C—O), 1088.73 cm^{-1} (O—H bending) and 833.96 cm^{-1} (C—C stretching) corresponds to PVA fibres (E-Suppl. Fig. 2). No change in the FTIR spectra was observed for the ML11 peptide encapsulated nanospun CS-PVA fibres and according to Ravikumar et al. [52] this is due to the weaker reflection of chitosan which may be because of the lower concentration of chitosan incorporated into the PVA solution. This was agreed with Kamble et al. [53] where, there was no changes in the shifting and no polymer-drug interaction was observed.

3.8.3. XRD analysis of ML11 peptide encapsulated nanofiber

The XRD pattern of the chitosan fibres shows a strong reflection at 19.79° and the PVA fibres shows a strong reflection at 19.36°, 22.38° and 40.45°. While, the ML11 peptide encapsulated nanospun fibres of CS-PVA shows a strong broad band which indicates the change in crystalline to amorphous behaviour. The change in the crystalline to amorphous nature is due to its strong interaction between CS and PVA during the blending process. The results exhibit the XRD pattern of CS, PVA, and CS-PVA of 1:3, 1.5:3 and 2:3 ratio fibres (E-Suppl. Fig. 3). Compared with the PVA fibres and CS fibres which reveals the

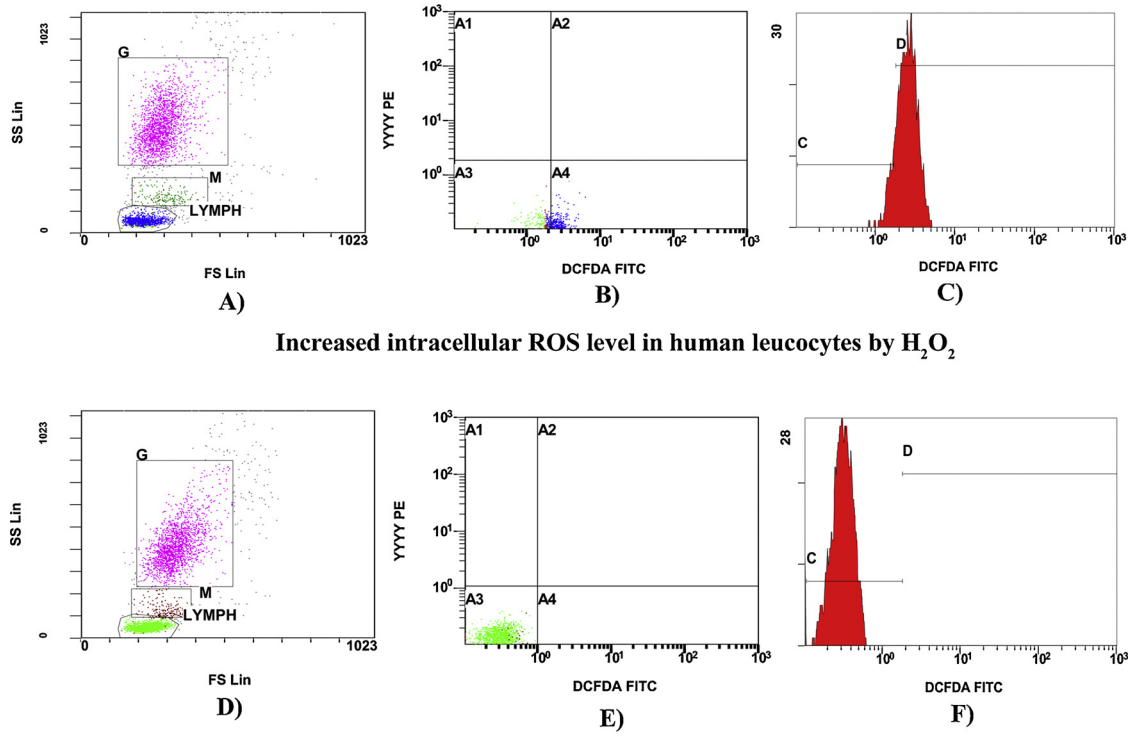

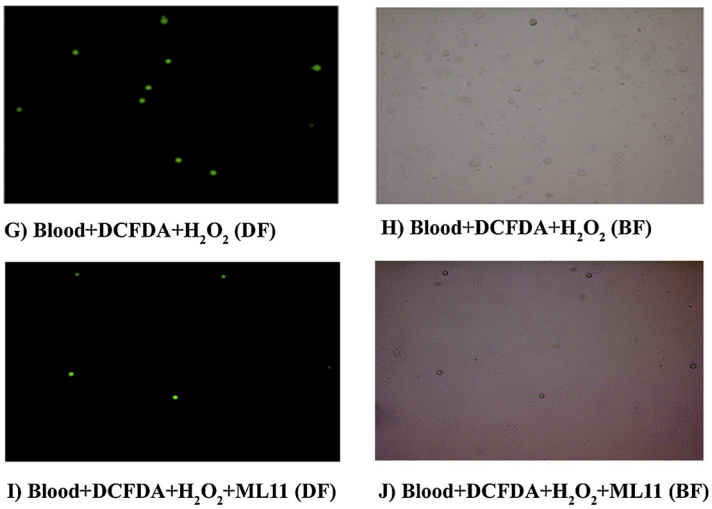

Fig. 3. Intracellular ROS quenching activity of ML11 peptide on human PBMCs. The level of intracellular ROS in PBMCs were assessed using FACS by fluorescent probe DCFDA: (A) Blood profile after 2 mM of H_2O_2 exposure; B) DCFDA fluorescence shift due to elevated levels of intracellular ROS; (C) Histogram displaying a strong fluorescence peak shift at 2 mM H_2O_2 exposure due to elevated level of ROS in PBMCs; (D) Blood profile after treated with H_2O_2 (2 mM) and ML11 peptide. (E) There was no fluorescence shift due to ML11 peptide ROS scavenging activity; (F) Histogram displaying no fluorescence peak shift due to low leucocytes ROS. Data represented is the mean ± SD (n = 3). Fluorescence imaging disclosed the level of intracellular ROS captured by Fluorescence microscopy: (G) Dark field image showing the fluorescence of ROS-DCFDA complex in leucocytes treated with H_2O_2; (H) Bright field image that shows the actual cells; (I) Dark field image with decreased level of intracellular ROS in ML11 treated peptide cells; (J) Bright field image that shows the actual cells. The scale bar of the light microscopic images (G, H, I and J) are 20 μm.

crystalline structure, the CS-PVA and CS-PVA-ML11 blends exhibits its amorphous structure. Jia et al, demonstrated that the change in crystalline to amorphous structure may be due to the fine solidification of polymers during the spinning process which halted the crystals formation [54].

3.9. Entrapment efficiency and release kinetics of ML11 peptide

Loading capacity of the peptide determines the *in vitro* release of peptide from nanofibrous mat by interaction of hydrophobic polymer and the drug which results in the controlled release [55]. The loading capacity of the ML11 peptide was measured to determine the amount of peptide that has been loaded completely into the nanofiber. The loading capacity of the peptide in nanofiber was observed to be at lower concentration (12 %). The obtained loading capacity was found to be indistinguishable where the loading capacity concentration was observed between 9.11–21.9 % [56].

To determine whether the electrospun nanofibers has entrapped the

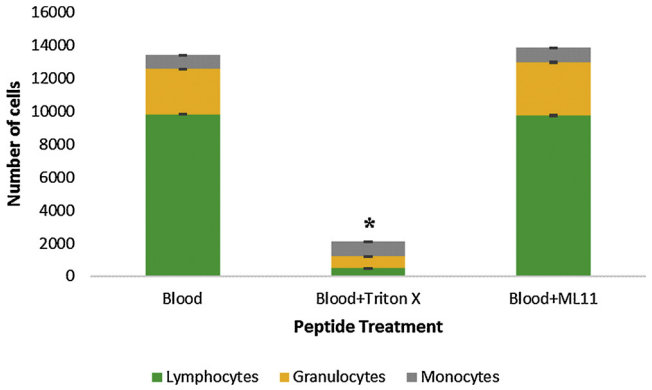

Fig. 4. Cell toxicity of ML11 on human blood leucocytes. ML11 cell toxicity was assessed against blood leucocytes when 100 μM ML11 peptide was present or absent. For positive and negative control, Triton X-100 and PBS was used, respectively. In blood leucocytes, ML11 peptide did not show any significant cell toxicity. Data represented is the mean ± SD (n = 3). The asterisk (*) indicates the significant difference between positive control (Triton X-100) and treatment (100 μM) by two-way ANOVA and Sidak's test in GraphPad prism (version 8.0.2).

peptide into the polymeric fibres, it was confirmed by entrapment efficiency. This study confirms the electrospinning method efficiency by maintaining the stability of peptide and to perform the controlled release of peptide from the nanofiber. The results showed that the ML11 peptide loaded CS-PVA entrapment efficiency was 76% which is agreed with the previous report, gentamicin loaded with PCL-collagen nanofiber and its entrapment efficiency was 81% [57]. The entrapment and loading efficiency of the peptide in nanofiber suggests that the value of electrospinning method in the effective controlled release of peptide.

The release kinetics of the ML11 peptide was evaluated to study the behaviour of peptide from the nanofibrous mat and the release was measured in cumulative percentage. The results showed that the cumulative amount of peptide was released from the ML11 peptide encapsulated mat (E-Suppl. Fig. 4A) and also a burst release of peptide was observed with 16 % at 1 h and it gradually increases with the time (E-Suppl. Fig. 4B). The release rate of peptide from the ML11 peptide encapsulated mat may be due to the release of peptide from the surface of the polymeric mat or from the degradation of the nanofiber [58]. The cumulative release was calculated for 10 h and at 10^{th} hour the release percent was 85 % cumulatively. After the 10^{th} hour, the concentration of peptide starts to saturate and on the 2nd day there was very less concentration left in the mat which confirms the peptide has been released out quickly and on the 3^{rd}day there was no release at all. As suggested by Gencturk et al, the initial burst and a quick release of peptide from the mat is most commonly due to the peptide which was on the surface of the fibre gets dissolved [59]. Also, the sustained release until the saturation is because of the peptide gets released from the pores of the polymeric mat.

3.10. Intracellular ROS scavenging activity of ML11 peptide encapsulated nanofiber

This study determines the amount of ROS level scavenged by the antioxidant peptide ML11 encapsulated mat. To determine the effect of antioxidant peptide ML11 in scavenging the ROS, the intracellular oxidative stress measurement was performed with help of DCFDA dye. The results showed that the ML11 peptide encapsulated mat has showed significant changes in the intracellular ROS level in the human leucocytes (Fig. 6A–C). Further, it was confirmed by confocal microscopy. The leucocytes treated with ML11 peptide encapsulated CS/PVA mat reveals reduced the fluorescence intensity significantly than the control CS/PVA mat (Fig. 6D–F). The reduction in the fluorescence intensity was observed in the peptide encapsulated mat treated leucocytes which strongly suggest that ML11 peptide encapsulated CS/PVA mat has potential ROS scavenging activity.

3.11. Cell viability assay

The cell viability activity of the ML11 peptide encapsulated mats were performed on NIH-3T3 mouse embryonic fibroblast cells. The findings exhibited that the ML11 peptide encapsulated nanofiber showed no significant toxicity against the NIH-3T3 cells and the viability of cells were observed between 90%–100% (Fig. 7A). Likewise, Mohamed et al, stated that the viability of NIH-3T3 cells treated with maltodextrin were 100 % [26]. Thus, the study was confirming that the ML11 peptide encapsulated mat showed more cell viability and the cells grew through the pores of the nanofibrous mat which further confirms the biocompatibility of the chitosan/PVA mat is suitable for the use in wound healing.

3.12. Effect of ML11 peptide encapsulated nanofiber on NIH-3T3 cells

Generally, the wound healing activity evaluated by the migration and proliferation of the fibroblasts [60]. *In vitro* scratch assay mimics the wound *in vivo* and to determine the rate of migration of cells in the presence of peptide. When the scratch is made the cell to lose its interaction with the other cell and it starts producing growth factors which initiate proliferation of cell and migration towards the scratch. The closure of scratch invitro demonstrates the wound healing activity of antioxidant peptide. The migration rate of the cells towards the scratch was fast and this is due to the stimulatory activity of peptide on the cells [27]. The effect of antioxidant peptide on the migration of cells was determined by performing scratch assay and the ability of the cells to undergo migration in the presence of the nanofibrous mat. Initially, cells were seeded at 8×10^5 cells/well and starved in incomplete media. The ML11 peptide encapsulated nanofibre wound closure activity was time dependent. The NIH-3T3 cells which has the fast proliferation rate started to proliferate at the zero hour itself in the control wells and the migration of the cells was observed in peptide treated as well. Scratch wound closure activity at 24 h time interval was observed to be 13.79%. Further, at 48 h time interval, the wound closure activity was noted to be 72.41% (Fig. 7B–E). Finally, at 72 h, the migration of the cells completely closed the wounded gap and the activity of wound closure was found to be 98.62 %. Overall, the study concludes that the antioxidant peptide ML11 encapsulated mat has a promising effect on the wound closure activity and this would be an efficient drug for the treatment of chronic wounds or skin ulcers.

4. Conclusion

An antioxidant peptide, ML11 has been derived from transglutaminase core domain of *A. platensis*, and its free radical scavenging potential has been demonstrated. ML11 did not show toxicity towards human blood leucocytes which indicates that the peptide has therapeutic potential. The ML11 encapsulated nanofiber mat retains the antioxidant activity by scavenging the intracellular ROS, this was demonstrated through flowcytometry and fluorescence microscopic analysis. Also, the peptide encapsulated mat showed no toxic effect on the NIH-3T3 mouse embryonic fibroblast cells; however, the peptide showed effective wound healing efficiency on the NIH-3T3 cells, insisting the curative property of ML11. Overall, the research shows that ML11 has antioxidant potential and that it is efficient in wound healing, thus the peptide possesses pharmacological benefits. Moreover, the ML11 peptide- CS-PVA nanofiber mat could be a promising biomaterial in restoring redox balance to promote wound healing.

Declaration of Competing Interest

The authors have declared that no competing interests exist.

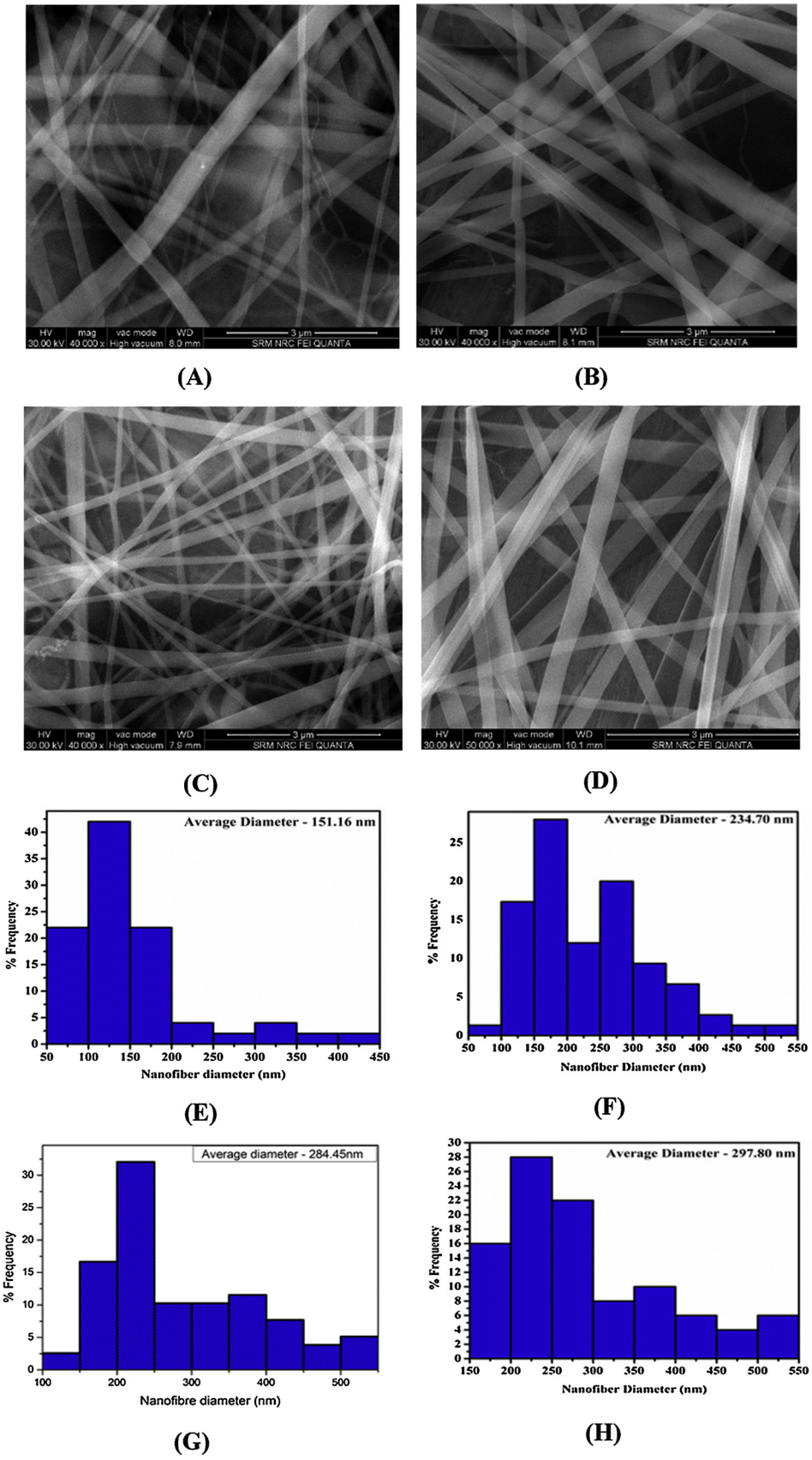

Fig. 5. FE-SEM analysis of ML11 encapsulated CS-PVA mat. (A) CS-PVA 1:3; (B) CS-PVA 1.5:3; (C) CS-PVA 2:3, which shows the randomly arranged and bead free structure fibers; (D) ML11 peptide encapsulated CS-PVA mat; (E) Fiber diameter distribution of 1:3 of CS-PVA; (F) Fiber diameter distribution of 1.5:3 of CS-PVA; (G) Fiber diameter distribution of 2:3 CS-PVA; (H) Fiber diameter of ML11 encapsulated CS-PVA (1.5:3) mat.

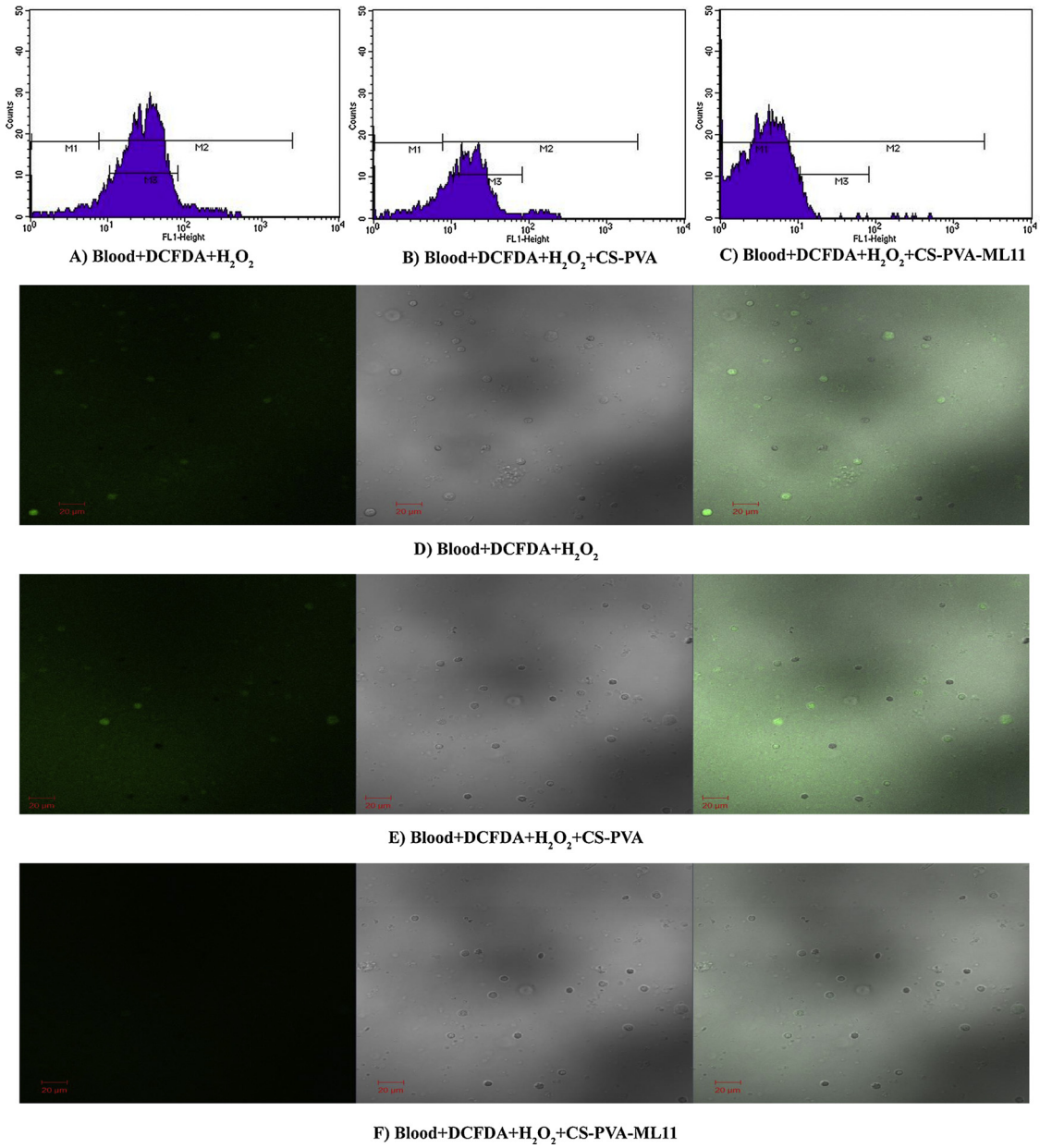

Fig. 6. Effect of ML 11 peptide encapsulated CS-PVA mat in reducing ROS. Reduction in the oxidative stress in human blood leucocytes were analysed by DCFDA dye using FACS analysis. (A) Histogram image depicts the shift in fluorescent confirms the increased level of oxidative stress in hydrogen peroxide treated leucocyte sample (B) Histogram image shows the reduced shift in fluorescent intensity confirms the reduced concentration level of oxidative stress in the CS-PVA mat treated leucocytes (C) Histogram image shows no shift in fluorescent intensity confirms the reduction in oxidative stress to a greater extent in the peptide treated leucocyte sample. All the data were shown in mean ± SD and n = 3. The confocal microscopy study revealed the reduction in the intracellular oxidative stress of leucocyte cells. (D) Dark field image illustrates the presence of oxidative stress in Hydrogen peroxide treated leucocytes cells *via* fluorescence intensity and bright field image illustrates the cells of leucocytes (E) Dark field image shows the slight reduction in the fluorescent intensity in the CS PVA control mats treated cell and the Bright field image illustrates the leucocyte cells (F) Dark field image illustrates no fluorescent intensity which confirms the reduced intracellular oxidative stress in the CS-PVA-ML11 mat treated cells and Bright field image shows the leucocyte cells. All the data were shown in mean ± SD and n = 3.

Informed consent

For Blood collection, informed consent was obtained from all the participated adults in written form.

Author agreement statement

The authors declare that this manuscript is original, has not been published before and is not currently being considered for publication elsewhere. We confirm that the manuscript has been read and approved by all named authors and that there are no other persons who satisfied the criteria for authorship but are not listed. We further confirm that the order of authors listed in the manuscript has been approved by all of us. We understand that the corresponding author is the sole contact for the editorial process. The corresponding author is responsible for communicating with the other authors about progress, submissions of revisions and final approval of proofs.

Acknowledgments

The authors would like to extend their sincere appreciation to the Deanship of Scientific Research at King Saud University, Riyadh, Saudi

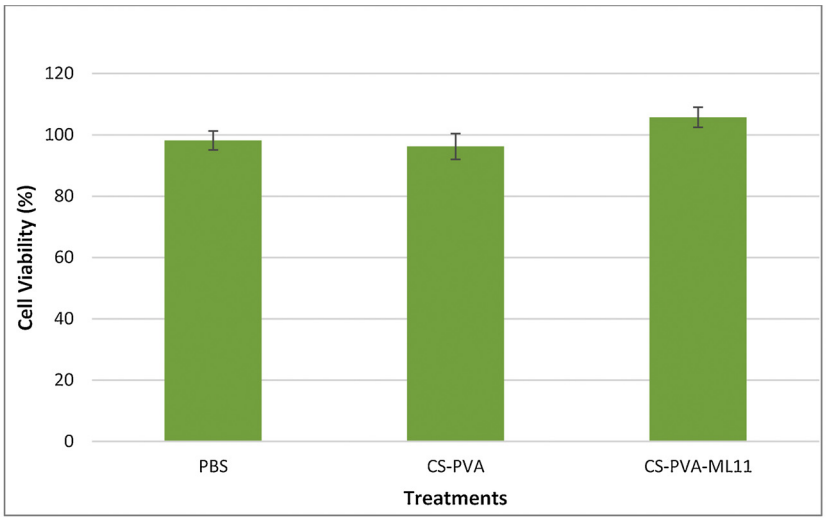

(A)

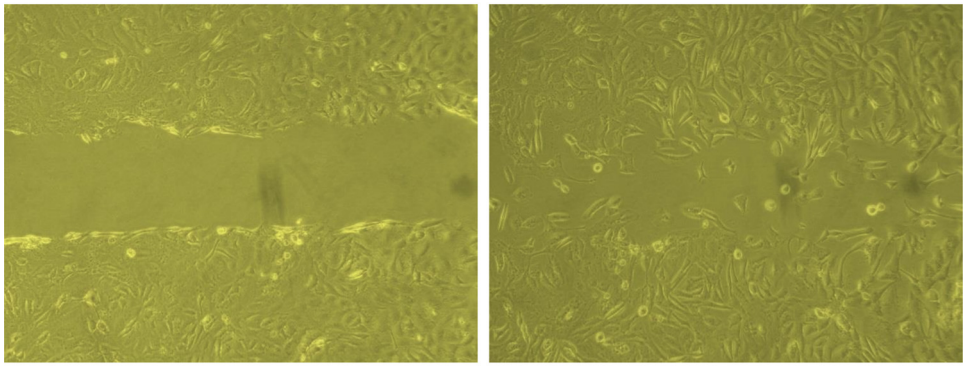

(B) (C)

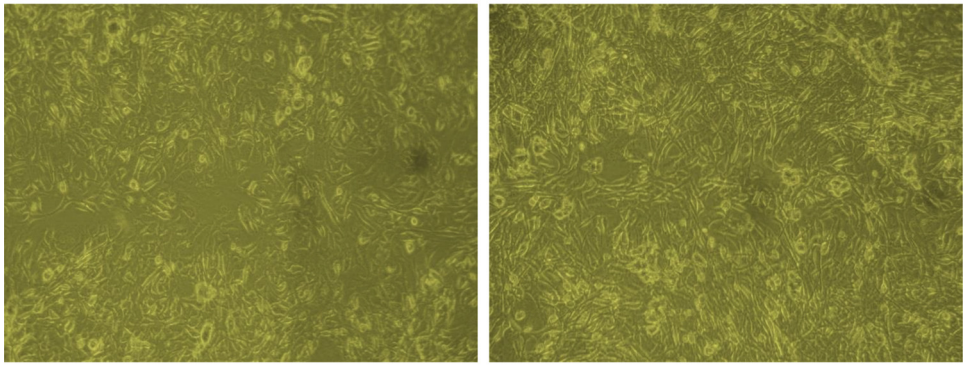

(D) (E)

Fig. 7. Effect of ML11 encapsulated CS-PVA mat on NIH-3T3 cells. NIH-3T3 cell proliferation and migration were evaluated in the mouse fibroblast using ML11 peptide treated and untreated mats; (A) The ML11 encapsulated CS-PVA mat determines the NIH-3T3 cell viability and proliferation. Phosphate buffer saline was used as control and ML11 peptide encapsulated CS-PVA mat showed no cytotoxic effect on the NIH-3T3 cells. The asterisk symbol (∗) signifies the control is statistically vary from the treatments. Data indicated as mean and standard deviation with the n value = 3 and the p value = < 0.05 was contemplated as significant. The proliferation and migration of the cells were observed after the scratch made on monolayer (B) Wounded cells at 0^{th} h (C) ML11 peptide treated mat at 24 h showed 13.79% closure activity (D) Peptide treated at 48 h revealed 72.41 % wound closure activity (E) Peptide treated cells at 72 h exhibited 98.62 % closure activity. The scale bar of the light microscopic images (B, C, D and E) are 20 μm.

Arabia for funding this Research Group Project (No. RGP-289). UPM contribution to the research is made possible through research grant LRGS/1/2019/UPM/1.

Appendix A. Supplementary data

Supplementary material related to this article can be found, in the online version, at doi:https://doi.org/10.1016/j.colsurfb.2020.111124.

References

[1] T. Kurahashi, J. Fujii, Roles of antioxidative enzymes in wound healing, J. Dev. Biol. 3 (2015) 57–70, https://doi.org/10.3390/jdb3020057.

[2] J.E. Janis, R.K. Kwon, D.H. Lalonde, A practical guide to wound healing, Plast. Reconstr. Surg. 125 (2010) 230–244, https://doi.org/10.1097/PRS.0b013e3181d9a0d1.

[3] R.M. El-Ferjani, M. Ahmad, S.M. Dhiyaaldeen, F.W. Harun, M.Y. Ibrahim, H. Adam, B. Mohd Yamin, M.M.J. Al-Obaidi, R. Al Batran, In vivo assessment of antioxidant and wound healing improvement of a new schiff base derived Co (II) complex in rats, Sci. Rep. 6 (2016) 1–12, https://doi.org/10.1038/srep38748.

[4] P. Zahedi, I. Rezaeian, S.O. Ranaei-Siadat, S.H. Jafari, P. Supaphol, A review on wound dressings with an emphasis on electrospun nanofibrous polymeric bandages, Polym. Adv. Technol. 21 (2010) 77–95, https://doi.org/10.1002/pat.1625.

[5] B. Poljšak, P. Jamnik, P. Raspor, M. Pesti, Oxidation-antioxidation-reduction processes in the cell: impacts of environmental pollution, Encycl. Environ. Heal. (2011) 300–306, https://doi.org/10.1016/b978-0-444-52272-6.00679-6.

[6] J. Kanta, The role of hydrogen peroxide and other reactive oxygen species in wound healing, Acta Medica (Hradec Kralove) 54 (2011) 97–101, https://doi.org/10.14712/18059694.2016.28.

[7] M. Wlaschek, K. Scharffetter-Kochanek, Oxidative stress in chronic venous leg ulcers, Wound Repair Regen. 13 (2005) 452–461, https://doi.org/10.1111/j.1067-1927.2005.00065.x.

[8] K. Tarun, N. Gobi, Calcium alginate/PVA blended nanofibre matrix for wound dressing, Indian J. Fibre Text. Res 37 (2012) 127–132.

[9] S.Z. Fu, X.H. Meng, J. Fan, L.L. Yang, Q.L. Wen, S.J. Ye, S. Lin, B.Q. Wang, L.L. Chen, J.B. Wu, Y. Chen, J.M. Fan, Z. Li, Acceleration of dermal wound healing by using electrospun curcumin-loaded poly(ε-caprolactone)-poly(ethylene glycol)-poly(ε-caprolactone) fibrous mats, J. Biomed. Mater. Res. - Part B Appl. Biomater. 102 (2014) 533–542, https://doi.org/10.1002/jbm.b.33032.

[10] S.F. Hosseini, Z. Nahvi, M. Zandi, Antioxidant peptide-loaded electrospun chitosan/poly(vinyl alcohol) nanofibrous mat intended for food biopackaging purposes, Food Hydrocoll. 89 (2019) 637–648, https://doi.org/10.1016/j.foodhyd.2018.11.033.

[11] N. Charernsriwilaiwat, T. Rojanarata, T. Ngawhirunpat, P. Opanasopit, Electrospun chitosan/polyvinyl alcohol nanofibre mats for wound healing, Int. Wound J. 11 (2014) 215–222, https://doi.org/10.1111/j.1742-481X.2012.01077.x.

[12] Y. Deldar, Y. Pilehvar-Soltanahmadi, M. Dadashpour, S. Montazer Saheb, M. Rahmati-Yamchi, N. Zarghami, An in vitro examination of the antioxidant, cytoprotective and anti-inflammatory properties of chrysin-loaded nanofibrous mats for potential wound healing applications, Artif. Cells, Nanomed. Biotechnol. 46 (2018) 706–716, https://doi.org/10.1080/21691401.2017.1337022.

[13] A. Sannasimuthu, V. Kumaresan, M. Pasupuleti, B.A. Paray, M.K. Al-Sadoon, J. Arockiaraj, Radical scavenging property of a novel peptide derived from C-terminal SOD domain of superoxide dismutase enzyme in Arthrospira platensis, Algal Res. 35 (2018) 519–529, https://doi.org/10.1016/j.algal.2018.09.028.

[14] V. Kumaresan, F. Nizam, G. Ravichandran, K. Viswanathan, R. Palanisamy, P. Bhatt, M.V. Arasu, N.A. Al-Dhabi, K. Mala, J. Arockiaraj, Transcriptome changes of blue-green algae, Arthrospira sp. in response to sulfate stress, Algal Res. 23 (2017) 96–103, https://doi.org/10.1016/j.algal.2017.01.012.

[15] A. Sannasimuthu, V. Kumaresan, S. Anilkumar, M. Pasupuleti, M.R. Ganesh, K. Mala, B.A. Paray, M.K. Al-Sadoon, M.F. Albeshr, J. Arockiaraj, Design and characterization of a novel Arthrospira platensis glutathione oxido-reductase-derived antioxidant peptide GM15 and its potent anti-cancer activity via caspase-9 mediated apoptosis in oral cancer cells, Free Radic. Biol. Med. 135 (2019) 198–209, https://doi.org/10.1016/j.freeradbiomed.2019.03.006.

[16] A. Sannasimuthu, J. Arockiaraj, Intracellular free radical scavenging activity and protective role of mammalian cells by antioxidant peptide from thioredoxin disulfide reductase of Arthrospira platensis, J. Funct. Foods 61 (2019) 103513, , https://doi.org/10.1016/j.jff.2019.103513.

[17] F. Bamdad, S. Ahmed, L. Chen, Specifically designed peptide structures effectively suppressed oxidative reactions in chemical and cellular systems, J. Funct. Foods 18 (2015) 35–46, https://doi.org/10.1016/j.jff.2015.06.055.

[18] B. Poljsak, D. Šuput, I. Milisav, Achieving the balance between ROS and antioxidants: when to use the synthetic antioxidants, Oxid. Med. Cell. Longev. 2013 (2013), https://doi.org/10.1155/2013/956792.

[19] Y. Liu, M. Park, H.K. Shin, B. Pant, S.J. Park, H.Y. Kim, Preparation and characterization of chitosan-based nanofibers by ecofriendly electrospinning, Mater. Lett. 132 (2014) 23–26, https://doi.org/10.1016/j.matlet.2014.06.041.

[20] K. Desai, K. Kit, J. Li, S. Zivanovic, Morphological and surface properties of electrospun chitosan nanofibers, Biomacromolecules 9 (2008) 1000–1006, https://doi.org/10.1021/bm701017z.

[21] A.A. Nada, A.G. Hassabo, A.L. Mohamed, S. Zaghloul, Encapsulation of nicotinamide into cellulose based electrospun fibers, J. Appl. Pharm. Sci. 6 (2016) 13–21, https://doi.org/10.7324/JAPS.2016.60803.

[22] F. Zamani, F. Jahanmard, F. Ghasemkhah, S. Amjad-Iranagh, R. Bagherzadeh, M. Amani-Tehran, M. Latifi, Nanofibrous and nanoparticle materials as drug-delivery systems, Nanostructures for Drug Delivery, Elsevier Inc., 2017, https://doi.org/10.1016/b978-0-323-46143-6.00007-5.

[23] E. Nagarajan, P. Shanmugasundaram, V. Ravichandiran, A. Vijayalakshmi, B. Senthilnathan, K. Masilamani, Development and evaluation of chitosan based polymeric nanoparticles of an antiulcer drug Lansoprazole, Int. J. Appl. Pharm. Sci. Res. 5 (2015) 20–25, https://doi.org/10.7324/JAPS.2015.50404.

[24] E. Eruslanov, S. Kusmartsev, Identification of ROS using DCFDA and flow-cytometry, Adv. Protoc. Oxidative Stress II 594 (2010) 57–72, https://doi.org/10.1007/978-1-60761-411-1.

[25] H.A. Rather, R. Thakore, R. Singh, D. Jhala, S. Singh, R. Vasita, Antioxidative study of Cerium Oxide nanoparticle functionalised PCL-Gelatin electrospun fibers for wound healing application, Bioact. Mater. 3 (2018) 201–211, https://doi.org/10.1016/j.bioactmat.2017.09.006.

[26] Z. Mohamed Amin, S.P. Koh, S.K. Yeap, N.S. Abdul Hamid, C.P. Tan, K. Long, Efficacy study of broken rice maltodextrin in in vitro wound healing assay, Biomed Res. Int. 2015 (2015), https://doi.org/10.1155/2015/687694.

[27] C. Vittorazzi, D.C. Endringer, T.U. De Andrade, R. Scherer, M. Fronza, Antioxidant, antimicrobial and wound healing properties of Struthanthus vulgaris, Pharm. Biol. 54 (2016) 331–337, https://doi.org/10.3109/13880209.2015.1040515.

[28] Y. Tsai, C.G. Lin, W.L. Chen, Y.C. Huang, C.Y. Chen, K.F. Huang, C.H. Yang, Evaluation of the antioxidant and wound-healing properties of extracts from different parts of hylocereus polyrhizus, Agronomy 9 (2019) 1–11, https://doi.org/10.3390/agronomy9010027.

[29] I. Han, H.J. Park, S.C. Seong, S. Lee, I.G. Kim, M.C. Lee, Role of transglutaminase 2 in apoptosis induced by hydrogen peroxide in human chondrocytes, J. Orthop. Res. 29 (2011) 252–257, https://doi.org/10.1002/jor.21241.

[30] J.M. Kim, A.M. Liceaga, K.Y. Yoon, Purification and identification of an antioxidant peptide from perilla seed (Perilla frutescens) meal protein hydrolysate, Food Sci. Nutr. 7 (2019) 1645–1655, https://doi.org/10.1002/fsn3.998.

[31] Y.L. Zhuang, X. Zhao, B.F. Li, Optimization of antioxidant activity by response surface methodology in hydrolysates of jellyfish (Rhopilema esculentum) umbrella collagen, J. Zhejiang Univ. Sci. B 10 (2009) 572–579, https://doi.org/10.1631/jzus.B0920081.

[32] H.L. Jang, A.M. Liceaga, K.Y. Yoon, Purification, characterisation and stability of an antioxidant peptide derived from sandfish (Arctoscopus japonicus) protein hydrolysates, J. Funct. Foods 20 (2016) 433–442, https://doi.org/10.1016/j.jff.2015.11.020.

[33] S. Ranathunga, N. Rajapakse, S.K. Kim, Purification and characterization of antioxidative peptide derived from muscle of conger eel (Conger myriaster), Eur. Food Res. Technol. 222 (2006) 310–315, https://doi.org/10.1007/s00217-005-0079-x.

[34] E. Nguyen, O. Jones, Y.H.B. Kim, F. San Martin-Gonzalez, A.M. Liceaga, Impact of microwave-assisted enzymatic hydrolysis on functional and antioxidant properties of rainbow trout Oncorhynchus mykiss by-products, Fish. Sci. 83 (2017) 317–331, https://doi.org/10.1007/s12562-017-1067-3.

[35] R. Re, N. Pellegrini, A. Proteggente, A. Pannala, M. Yang, C. Rice-Evans, Antioxidant activity applying an improved ABTS radical cation decolorization assay, Free Radic. Biol. Med. 26 (1999) 1231–1237, https://doi.org/10.1016/S0891-5849(98)00315-3.

[36] C. Aliaga, E.A. Lissi, Reaction of 2,2′-azinobis 3-ethylbenzothiazoline-6-sulfonic acid (ABTS) derived radicals with hydroperoxides. Kinetics and mechanism, Int. J. Chem. Kinet. 30 (1998) 565–570, https://doi.org/10.1002/(SICI)1097-4601(1998)30:8<565::AID-KIN5>3.0.CO;2-Q.

[37] S. Ketnawa, M. Wickramathilaka, A.M. Liceaga, Changes on antioxidant activity of microwave-treated protein hydrolysates after simulated gastrointestinal digestion: purification and identification, Food Chem. (2018), https://doi.org/10.1016/j.foodchem.2018.01.133.

[38] H. Zhuang, N. Tang, Y. Yuan, Purification and identification of antioxidant peptides from corn gluten meal, J. Funct. Foods 5 (2013) 1810–1821, https://doi.org/10.1016/j.jff.2013.08.013.

[39] K. Zhu, H. Zhou, H. Qian, Antioxidant and free radical-scavenging activities of wheat germ protein hydrolysates (WGPH) prepared with alcalase, Process Biochem. 41 (2006) 1296–1302, https://doi.org/10.1016/j.procbio.2005.12.029.

[40] M. Ohata, S. Uchida, L. Zhou, K. Arihara, Antioxidant activity of fermented meat sauce and isolation of an associated antioxidant peptide, Food Chem. 194 (2016) 1034–1039, https://doi.org/10.1016/j.foodchem.2015.08.089.

[41] C.Z. Zhu, W.G. Zhang, G.H. Zhou, X.L. Xu, Z.L. Kang, Y. Yin, Isolation and identification of antioxidant peptides from Jinhua ham, J. Agric. Food Chem. 61 (2013) 1265–1271, https://doi.org/10.1021/jf3044764.

[42] L.S. Wang, J.C. Huang, Y.L. Chen, M. Huang, G.H. Zhou, Identification and characterization of antioxidant peptides from enzymatic hydrolysates of duck meat, J. Agric. Food Chem. 63 (2015) 3437–3444, https://doi.org/10.1021/jf506120w.

[43] S.Y. Wang, M.J. Camp, M.K. Ehlenfeldt, Antioxidant capacity and α-glucosidase inhibitory activity in peel and flesh of blueberry (Vaccinium spp.) cultivars, Food Chem. 132 (2012) 1759–1768, https://doi.org/10.1016/j.foodchem.2011.11.134.

[44] P.A. Southorn, G. Powis, Free Radicals in Medicine. I. Chemical Nature and Biologic Reactions, Mayo Clin. Proc. 63 (1988) 381–389, https://doi.org/10.1016/S0025-6196(12)64861-7.

[45] R.J. Elias, S.S. Kellerby, E.A. Decker, Antioxidant activity of proteins and peptides, Crit. Rev. Food Sci. Nutr. 48 (2008) 430–441, https://doi.org/10.1080/10408390701425615.

[46] E. Escudero, M.C. Aristoy, H. Nishimura, K. Arihara, F. Toldrá, Antihypertensive effect and antioxidant activity of peptide fractions extracted from Spanish dry-cured ham, Meat Sci. 91 (2012) 306–311, https://doi.org/10.1016/j.meatsci.2012.02.008.

[47] L.J. Xing, Y.Y. Hu, H.Y. Hu, Q.F. Ge, G.H. Zhou, W.G. Zhang, Purification and identification of antioxidative peptides from dry-cured Xuanwei ham, Food Chem. 194 (2016) 951–958, https://doi.org/10.1016/j.foodchem.2015.08.101.

[48] S.J. Lee, Y.S. Kim, J.W. Hwang, E.K. Kim, S.H. Moon, B.T. Jeon, Y.J. Jeon, J.M. Kim, P.J. Park, Purification and characterization of a novel antioxidative peptide from duck skin by-products that protects liver against oxidative damage, Food Res. Int. 49 (2012) 285–295, https://doi.org/10.1016/j.foodres.2012.08.017.

[49] A.L. Miranda-Vilela, P.C.Z. Alves, A.K. Akimoto, L.C.S. Pereira, M. Nazaré Klautau-Guimarães, C.K. de Grisolia, The effect of hydrogen peroxide-induced oxidative stress on leukocytes depends on age and physical training in healthy human subjects carrying the same genotypes of antioxidant enzymes' gene polymorphisms, Am. J. Hum. Biol. 22 (2010) 807–812, https://doi.org/10.1002/ajhb.21086.

[50] Y.J. Gordon, E.G. Romanowski, A.M. McDermott, Mini review: a review of antimicrobial peptides and their therapeutic potential as anti-infective drugs, Curr. Eye Res. 30 (2005) 505–515, https://doi.org/10.1080/02713680590968637.

[51] D.I. Sanchez-Alvarado, J. Guzmán-Pantoja, U. Páramo-García, A. Maciel-Cerda, R.D. Martínez-Orozco, R. Vera-Graziano, Morphological study of chitosan/poly(vinyl alcohol) nanofibers prepared by electrospinning, collected on reticulated vitreous carbon, Int. J. Mol. Sci. 19 (2018) 1–12, https://doi.org/10.3390/ijms19061718.

[52] R. Ravikumar, M. Ganesh, U. Ubaidulla, E. Young Choi, H. Tae Jang, Preparation, characterization, and in vitro diffusion study of nonwoven electrospun nanofiber of curcumin-loaded cellulose acetate phthalate polymer, Saudi Pharm. J. 25 (2017) 921–926, https://doi.org/10.1016/j.jsps.2017.02.004.

[53] R.N. Kamble, S. Gaikwad, A. Maske, S.S. Patil, Fabrication of electrospun nanofibres of BCS II drug for enhanced dissolution and permeation across skin, J. Adv. Res. 7 (2016) 483–489, https://doi.org/10.1016/j.jare.2016.03.009.

[54] Y.T. Jia, H.Y. Kim, J. Gong, D.R. Lee, Electrospun nanofibers of block copolymer of trimethylene carbonate and ε-caprolactone, J. Appl. Polym. Sci. 99 (2006) 1462–1470, https://doi.org/10.1002/app.22633.

[55] H. Zhou, X. Liu, F. Wu, J. Zhang, Z. Wu, H. Yin, H. Shi, Preparation, characterization, and antitumor evaluation of electrospun resveratrol loaded nanofibers, J.

Nanomater. 2016 (2016), https://doi.org/10.1155/2016/5918462.
[56] H. Yang, K. Feng, P. Wen, M.H. Zong, W.Y. Lou, H. Wu, Enhancing oxidative stability of encapsulated fish oil by incorporation of ferulic acid into electrospun zein mat, LWT - Food Sci. Technol. 84 (2017) 82–90, https://doi.org/10.1016/j.lwt.2017.05.045.
[57] W.K.W. Abdul Khodir, A.H. Abdul Razak, M.H. Ng, V. Guarino, D. Susanti, Encapsulation and characterization of gentamicin sulfate in the collagen added electrospun nanofibers for skin regeneration, J. Funct. Biomater. 9 (2018) 36, https://doi.org/10.3390/jfb9020036.
[58] M.A. Zarandi, P. Zahedi, I. Rezaeian, A. Salehpour, M. Gholami, B. Motealleh, Drug release, cell adhesion and wound healing evaluations of electrospun carboxymethyl chitosan/polyethylene oxide nanofibres containing phenytoin sodium and Vitamin C, IET Nanobiotechnol. 9 (2015) 191–200, https://doi.org/10.1049/iet-nbt.2014.0030.
[59] A. Gencturk, E. Kahraman, S. Güngör, G. Özhan, Y. Özsoy, A.S. Sarac, Polyurethane/hydroxypropyl cellulose electrospun nanofiber mats as potential transdermal drug delivery system: characterization studies and in vitro assays, Artif. Cells, Nanomed. Biotechnol. 45 (2017) 655–664, https://doi.org/10.3109/21691401.2016.1173047.
[60] O.T. Agar, M. Dikmen, N. Ozturk, M.A. Yilmaz, H. Temel, F.P. Turkmenoglu, Comparative studies on phenolic composition, antioxidant, wound healing and cytotoxic activities of selected achillea L. Species growing in Turkey, Molecules 20 (2015) 17976–18000, https://doi.org/10.3390/molecules201017976.